Open Access Article. Published on 24 April 2025. Downloaded on 2/23/2026 1:20:25 PM.
This article is licensed under a Creative Commons Attribution-NonCommercial 3.0 Unported Licence.

Chemical Science

ROYAL SOCIETY OF CHEMISTRY

EDGE ARTICLE

View Article Online
View Journal | View Issue

Check for updates

Cite this: *Chem. Sci.*, 2025, **16**, 9413

All publication charges for this article have been paid for by the Royal Society of Chemistry

Tandem reaction-powered near-infrared fluorescent molecular reporter for real-time imaging of lung diseases†

Yan Hu,‡[a] Hongshuai Zhang,‡[a] Yiteng Ding,‡[a] Weirui Chen,[a] Changqie Pan,*[e] Longwei He, *[bc] Dan Cheng *[ac] and Lin Yuan [d]

Received 25th February 2025
Accepted 22nd April 2025

DOI: 10.1039/d5sc01488c

rsc.li/chemical-science

Diabetes and its complications have drawn growing research attention due to their detrimental effects on human health. Although optical probes have been used to help understand many aspects of diabetes, the lung diseases caused by diabetes remain unclear and have rarely been explored. Herein, a tandem-reaction (TR) strategy is proposed based on the adjacent diol esterification-crosslinking reaction and the nicotinamide reduction reaction of nicotinamide adenine dinucleotide (NADH) to design a lung-targeting near-infrared (NIR) small molecule probe (**NBON**) for accurate imaging of diabetic lung diseases. **NBON** was designed by coupling a phenylboronic acid analog that can form borate ester bonds by reversibly binding with NADH *via* an esterification-crosslinking reaction. Streptozotocin (STZ)-induced diabetic mice and metformin (MET)/epalrestat (EPS)-repaired model studies demonstrated that **NBON** allowed the sensitive imaging of NADH for lung disease diagnosis and therapeutic monitoring. The proposed antioxidant mechanism by which EPS alleviates diabetic lung disease was studied for the first time in living cells and *in vivo*. Furthermore, **NBON** was successfully applied in the detection of NADH in tumors and lung metastases. Overall, this work provides a general platform for a NIR NADH probe design, and advances the development of NADH probes for mechanistic studies in lung diseases.

Introduction

Diabetes mellitus is a metabolic disorder that is characterized by chronic hyperglycemia and which leads to multiple systemic diseases, rendering it one of the main causes of human death.[1,2] Indeed, the probabilities of premature death and functional disability are known to be higher in diabetic patients than in healthy individuals. The pathophysiological process of diabetes involves multiple organs, such as the liver and the kidneys.[3] In the 1970s, Schuyler *et al.* first proposed that the lungs may be one of the target organs of diabetic injury.[4] Since patients with diabetes are often in a state of hyperglycemia for long periods of time, a series of changes can be induced in the lungs, causing various lung diseases, such as pneumonia, pulmonary interstitial fibrosis, and lung cancer, among others.[5,6] Thus, the growing incidence rates of diabetes in recent decades poses a significant threat to human health.

Diabetes originates from glucose metabolism disorders and is characterized by sustained high blood sugar levels, which can lead to glucose toxicity. Nicotinamide adenine dinucleotide (NADH) is the most important coenzyme in cells, and is involved in substance and energy metabolism.[7] Because glucose is one of the main sources of NADH, its accumulation often leads to the excessive production of NADH, resulting in an intracellular NAD^+/NADH redox imbalance. During the entry of upregulated NADH electrons into the electron transfer chain, electrons may leak and bind to oxygen, producing a large amount of reactive oxygen species (ROS), thereby inducing oxidative stress, and ultimately leading to cell death.[8] Despite this knowledge, the specific regulatory mechanism of NADH in diabetes-induced lung diseases and the relationship between NADH levels and lung injury remain controversial. One of the main obstacles hindering the study of these molecular events is a lack of precise methods for the non-invasive detection of NADH concentration changes in cells, tissues, and *in vivo*. It is therefore desirable to construct a highly sensitive and selective

---

[a] *Department of Gastroenterology, The Affiliated Nanhua Hospital, Hengyang Medical School, University of South China, Hengyang 421002, Hunan, China. E-mail: flychand0110@163.com*

[b] *MOE Key Lab of Rare Pediatric Diseases, Hunan Province Cooperative Innovation Center for Molecular Target New Drug Study, Department of Pharmacy and Pharmacology, Hengyang Medical School, University of South China, Hengyang, China. E-mail: helongwei0110@163.com*

[c] *School of Chemistry and Chemical Engineering, Henan Normal University, Xinxiang, 453007, P. R. China*

[d] *State Key Laboratory of Chemo and Biosensing, College of Chemistry and Chemical Engineering, Hunan University, Changsha 410082, P. R. China*

[e] *Department of Thoracic Oncology, Hunan Cancer Hospital/The Affiliated Cancer Hospital of Xiangya School of Medicine, Central South University, Changsha, 410013, China. E-mail: panchangqie@hnca.org.cn*

† Electronic supplementary information (ESI) available. See DOI: https://doi.org/10.1039/d5sc01488c

‡ These authors contributed equally to this work.

© 2025 The Author(s). Published by the Royal Society of Chemistry

Open Access Article. Published on 24 April 2025. Downloaded on 2/23/2026 1:20:25 PM. This article is licensed under a Creative Commons Attribution-NonCommercial 3.0 Unported Licence.

fluorescent reporter to monitor NADH levels in diabetes-induced lung disease *in vivo*.

In recent years, with the rapid development of molecular imaging technologies, optical probes have attracted increasing attention owing to their high sensitivities, high spatial resolutions, rapid analysis, and noninvasive nature.[9–24] Consequently, they have become a powerful tool for the real-time monitoring and imaging of diabetes and lung diseases. To date, a number of NADH probes have been reported.[25–31] For example, Chang *et al.* developed a highly sensitive NADH probe inspired by enzyme-catalyzed reactions to detect NADH in living cells.[25] In addition, Kim *et al.* selected a rhodamine dye as the fluorescent group and constructed an NADH probe using the reducing ability of NAD(P)H to detect NAD(P)H during cellular hypoxia.[28] Furthermore, Yin *et al.* designed an NADH fluorescent probe using rhodamine dye to distinguish p53-abnormal tumors from normal tumors.[30] Although there has been some progress in the detection of NADH in cells using existing molecular fluorescent probes, the majority of advances have been achieved in situations where the concentration of NADH changes dramatically owing to human stimulation, rather than reflecting true fluctuations during pathological processes in living cells. As a result, these developed probes cannot provide accurate information regarding intracellular molecular events. In addition, the imaging wavelengths of most probes are relatively short, and significant improvements are required in terms of their sensitivities. Furthermore, considering that the lungs are located deep within the human body, issues related to probe targeting, spontaneous fluorescence interference and the imaging signal-to-noise (S/N) ratio must be addressed to successfully conduct noninvasive optical imaging *in vivo*. Owing to the ability of near-infrared (NIR) fluorescence imaging to detect the light emission of fluorescent dyes in the range of 650–900 nm, the spontaneous fluorescence of biological tissues in this range is significantly reduced, resulting in reduced light scattering.[32–47] Therefore, the development of NIR NADH fluorescence probes would be expected to permit the non-invasive *in vivo* imaging and detection of diabetic lung diseases with a high S/N ratio and a high sensitivity, thereby enhancing the accuracy and reliability of analysis and detection.

Herein, a tandem-reaction (TR) strategy is developed based on the adjacent diol esterification-crosslinking reaction and nicotinamide reduction reaction of NADH by introducing both an NADH recognition group and an NADH crosslinking group on the probe. This method is aimed at improving the probe sensitivity, whilst also promoting its specific targeting and accumulation in the lungs. A NIR semi-cyanine dye derivative is selected as the fluorescent reporting group, and hydroxyl protection and deprotection strategies are employed on the probe to achieve fluorescence regulation with the aim of constructing a highly sensitive lung-targeted NIR NADH probe (**NBON**). Subsequently, the developed probe is applied in the detection of endogenous NADH changes in cells, and to visualize trace fluctuations of the NADH levels in cells under high glucose stimulation conditions. The ability of the probe to visualize changes in the NADH levels in streptozotocin-induced diabetic lung diseases and in a metformin (MET)/epalrestat (EPS) repair model *in vivo* is also evaluated. Furthermore, antioxidant mechanism by which EPS alleviates diabetic lung disease is examined *in vivo*. Moreover, the developed probe is employed to sensitively detect changes in the NADH levels in lung tumors and metastases.

Results and discussion

Design and synthesis of NBON probe

NADH is a reducing agent composed of adenine, sugars (*ortho*-dihydroxyl compounds), phosphate linkers, and niacinamide (Fig. S1†). Its reduction mainly originates from the niacinamide site, which is often employed as the reactive attack site for NADH probes. However, the sensitivities of traditional NADH probes are often limited (Scheme 1A), and so an alternative approach should be considered. In this context, NADH contains an adjacent diol structure which is prone to reactions with phenylboronic acids. Inspired by this reaction, a TR strategy was considered for the design of a novel NADH probe (Scheme 1B). More specifically, a group containing a phenylboronic acid analog was initially attached onto the probe molecule to promote an esterification-crosslinking reaction with adjacent diols on NADH (Reaction 1). Subsequently, the recognition group on the probe molecule was modified for reduction by NADH, rendering it highly reactive (Reaction 2). Based on the above design idea, a highly stable semi-cyanine NIR dye derivative with a tunable hydroxy group was selected as the fluorescence reporting unit (CS), which exhibits a high fluorescence quantum yield and long absorption and emission wavelengths in the NIR region ($\lambda_{abs}/\lambda_{em} = 700/721$ nm).[48] Consequently, changes in the fluorescence signal can be regulated by protection and deprotection of the hydroxyl group. For this molecular structure, a long-chain phenylboronic acid binding group was introduced (NBCS) to impart the compound with a good hydrophilicity and promote effective circulation in the blood and accumulation in lungs.[49] Furthermore, compared to commercial MitoTracker Deep Red (Fig. S2 and S3†), NBCS exhibits a good photostability in solution and in cells, which is beneficial for biological imaging of the lung *in vivo*. For the NADH recognition group, a quinoline salt derivative was selected, and the target **NBON** was prepared (Scheme 1C). A control compound without the modified boronic acid binding group was also synthesized (NCCN), as outlined in Schemes 1C and S1.† Compounds were characterized by nuclear magnetic resonance (NMR) spectroscopy, mass spectrometry and high-performance liquid chromatography (HPLC), as detailed in the ESI.†

Optical properties of fluorescent probes toward NADH

Initially, the feasibility of **NBON** to detect NADH in a buffer solution (phosphate buffered saline (PBS)/ethanol (EtOH) = 7 : 3, pH 7.4) was investigated. As shown in Fig. 1A, the fluorescence spectrum indicated that **NBON** exhibited a sensitive response toward NADH (0–1 μM), with a 45 nM detection limit (Fig. 1B). In contrast, the control compound NCCN, which did not contain the long-chain phenylboronic acid binding group, showed no obvious signal changes in the presence of NADH (0–1 μM) under comparable conditions (Fig. 1C). It was speculated that this may have been caused by the low sensitivity of NCCN toward NADH. Indeed, in the presence of a higher NADH concentration (0–100 μM) (Fig. 1D), a relatively poor

© 2025 The Author(s). Published by the Royal Society of Chemistry

Open Access Article. Published on 24 April 2025. Downloaded on 2/23/2026 1:20:25 PM.
This article is licensed under a Creative Commons Attribution-NonCommercial 3.0 Unported Licence.

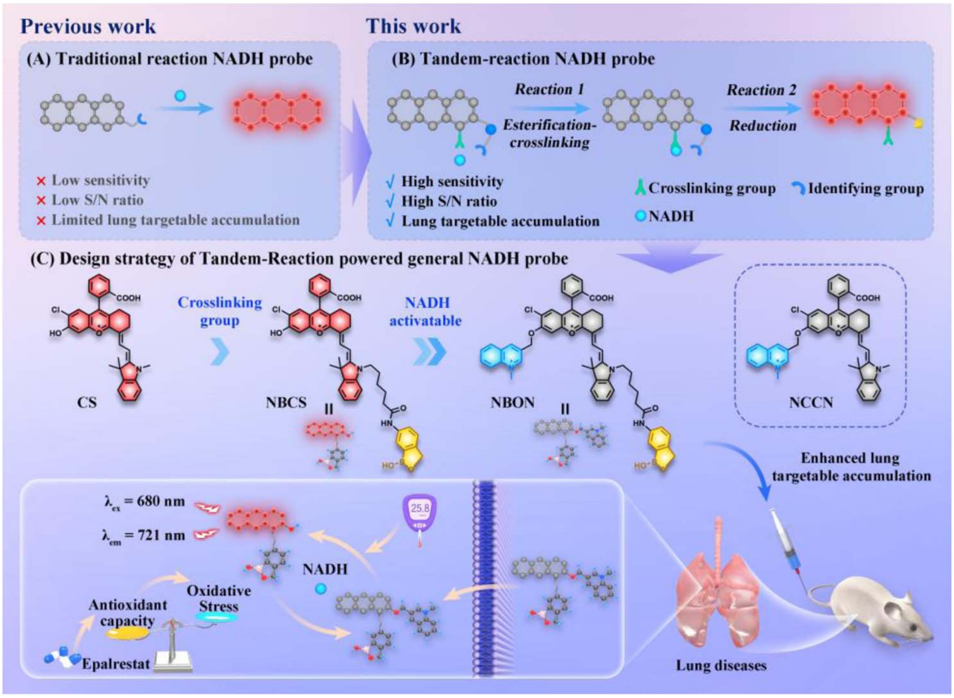

Scheme 1 (A) Traditional "reaction type" probes for NADH from previous work. (B) Our "tandem-reaction" type probes for NADH in this work. (C) Design and structure of compounds **NBON**/NCCN and the proposed mechanism of **NBON** for imaging NADH in diabetic lung diseases.

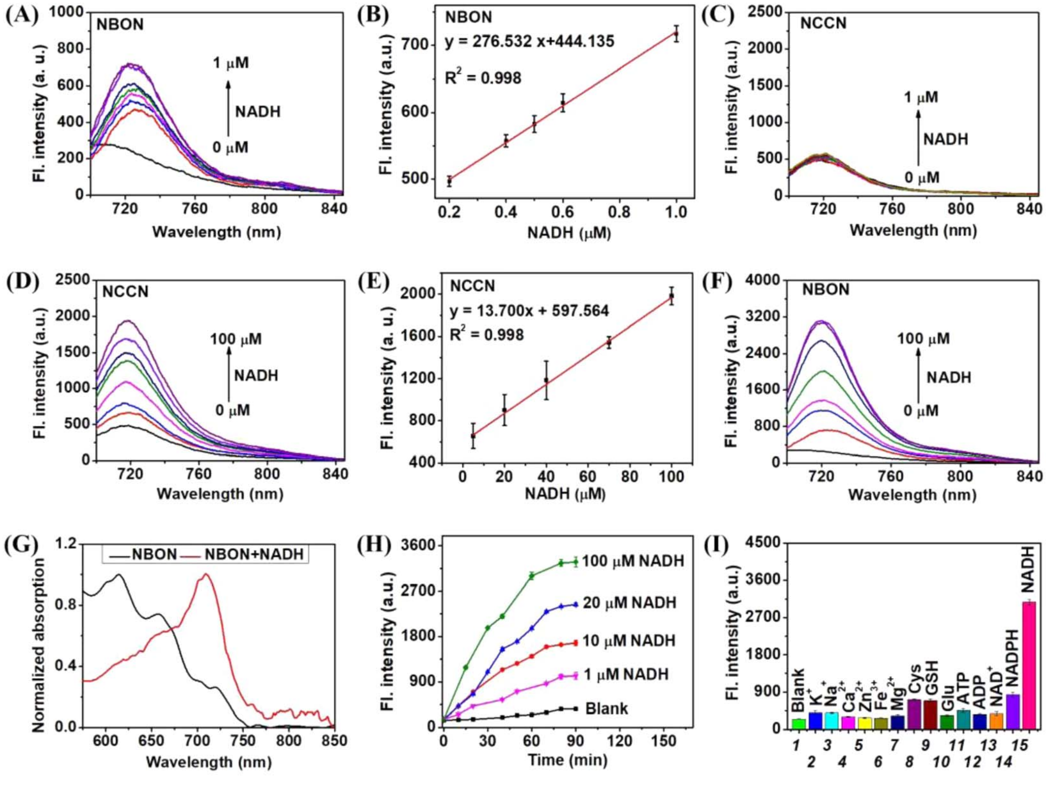

Fig. 1 (A) Fluorescence emission spectra of **NBON** (5 μM) with concentration of NADH (0–1 μM). (B) Linear correlation between the fluorescence intensity of **NBON** (5 μM) and NADH concentration. (C) Fluorescence emission spectra of NCCN (5 μM) with concentration of NADH (0–1 μM). (D) Fluorescence emission spectra of NCCN (5 μM) with concentration of NADH (0–100 μM). (E) Linear correlation between the fluorescence emission intensity of NCCN (5 μM) and NADH concentration. (F) Fluorescence emission spectra of **NBON** (5 μM) with concentration of NADH (0–100 μM). (G) Normalized absorption spectra of **NBON** (5 μM) in the presence of NADH (70 μM). (H) The time-dependent fluorescence intensity of **NBON** (5 μM) with NADH. (I) Fluorescence intensities of **NBON** to various analytes (2–7, 1 mM; 8–13, 100 μM; 14–15, 70 μM).

Open Access Article. Published on 24 April 2025. Downloaded on 2/23/2026 1:20:25 PM.
This article is licensed under a Creative Commons Attribution-NonCommercial 3.0 Unported Licence.

fluorescence enhancement was observed (Fig. S4†), and the detection limit was determined to be 2.5 μM (Fig. 1E), confirming the low sensitivity of this system. Thus, the detection of NADH by **NBON** was further evaluated upon increasing the NADH concentration to 100 μM. Notably, an apparent enhanced NIR signal ($\lambda_{em} = 721$ nm) was captured with a 12-fold increase in fluorescence intensity (Fig. 1F), while the absorption peak at 615/657 nm was red-shifted to 669/709 nm in response to NADH (Fig. 1G). These differences were attributed to the superior sensitivity of the **NBON** probe toward NADH (Table S1†), which in turn was caused by the presence of a phenylboronic acid binding group enabling a rapid response.

To further verify the reaction mechanism between **NBON** and NADH, high-performance liquid chromatography (HPLC)-mass spectrometry (MS) and mass spectrometry were performed. As shown in the HPLC-MS results presented in Fig. S5,† **NBON** (*m*/*z* 924.4, $[M]^+$) exhibited a single sharp characteristic peak with a retention time of 8.60 min. However, upon the addition of NADH, a new peak appeared with a retention time of 10.41 min, which was confirmed to originate from the expected product NBCS (*m*/*z* 767.3, $[M-H]^- = 767.3$). A compound I (*m*/*z* 1572.45, $[M]^+$) was also detected in the reaction mixture by mass spectrometry, which likely originated from the NADH response intermediate (Fig. S6†). The absorption spectra further supported the above results (Fig. S7†), thereby confirming the complete conversion of **NBON** to NBCS upon the reduction of NADH. This is consistent with the proposed reaction mechanism, and supports the design idea that **NBON** efficiently reacts with NADH *via* a TR strategy (Scheme S2†).

Subsequently, the fluorescence kinetic curves were recorded for **NBON** upon incubation with NADH (0–100 μM) for different incubation times (0–90 min). No apparent signal changes were observed in the absence of NADH (Fig. 1H); however, the fluorescence intensity of **NBON** increased rapidly after incubation with different NADH concentrations, and reached a plateau after 60 min, thereby suggesting that **NBON** can sensitively and rapidly detect changes in the NADH concentration. Furthermore, the selectivity of **NBON** toward NADH was investigated in the presence of various ions (Ca^{2+}, K^+, Na^+, Zn^{2+}, Fe^{2+}, and Mg^{2+}), reactive species (Cysteine (Cys) and glutathione (GSH)), and biomolecules (Glucose (Glu), adenosine triphosphate (ATP), adenosine diphosphate (ADP), nicotinamide adenine dinucleotide (NAD^+), and nicotinamide adenine dinucleotide phosphate (NADPH)). As shown in Fig. 1I, none of the other species responded to **NBON**, indicating the excellent selectivity of **NBON** toward NADH. In addition, it possessed a good photostability (Fig. S8†), and it was observed that **NBON** could successfully

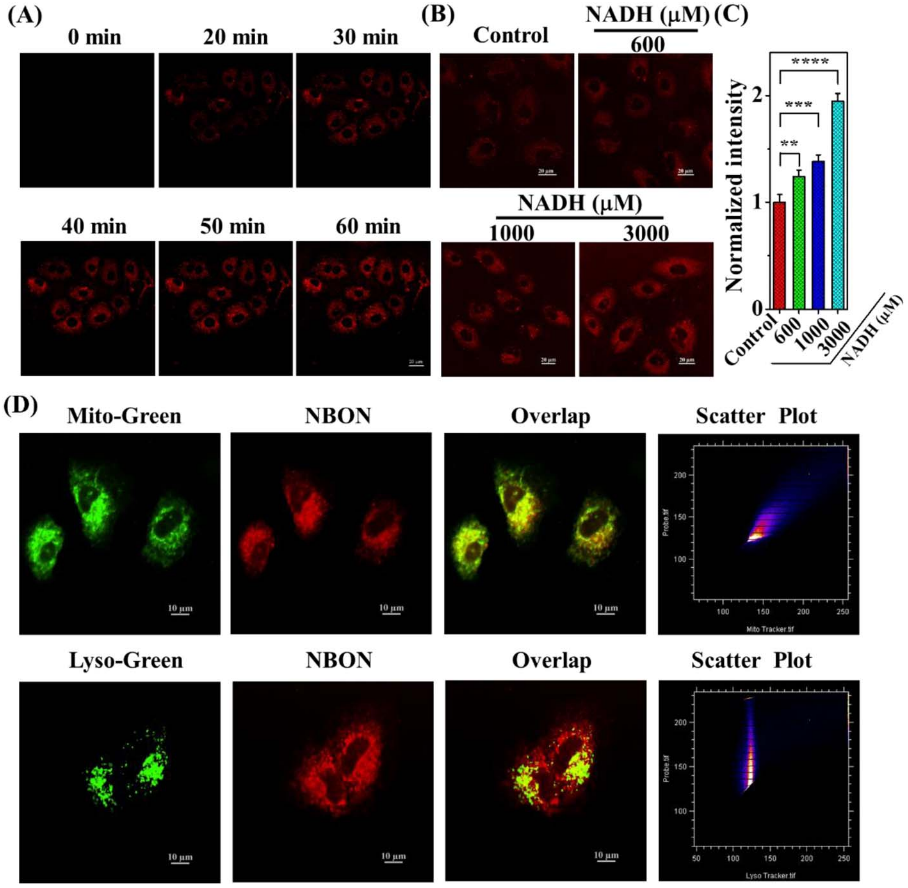

Fig. 2 (A) Fluorescence images of endogenous NADH in A549 cells incubated with **NBON** (15 μM) within 60 min. (B) Fluorescence images of exogenous NADH in A549 cells incubated with different concentration NADH (0–3000 μM) for 2 h, then incubated with **NBON** (15 μM) for 40 min. (C) Average fluorescence intensity in (B) ($n = 4$, data expressed as mean ± SD, $^{**}P < 0.01$, $^{***}P < 0.001$, and $^{****}P < 0.0001$, Student's *t*-test). Scale bar = 20 μm. (D) Intracellular localization of **NBON** in A549 cells using MitoTracker Green and LysoTracker Green. Scale bar: 10 μm.

© 2025 The Author(s). Published by the Royal Society of Chemistry

Open Access Article. Published on 24 April 2025. Downloaded on 2/23/2026 1:20:25 PM.
This article is licensed under a Creative Commons Attribution-NonCommercial 3.0 Unported Licence.

monitor NADH between pH 6.0 and 8.0 (Fig. S9†) upon variation in the solution pH, thereby confirming that **NBON** is a suitable agent for recognizing NADH in complex systems.

Fluorescence imaging of NADH in living cells using the NBON probe

Inspired by the above experiments performed using a buffer solution, the ability of **NBON** to detect NADH was evaluated in human lung cancer A549 cells overexpressing NADH. Initially, a MTT assay was conducted for 24 h using different **NBON** concentrations to confirm the low cytotoxicity of **NBON** toward the living cells (Fig. S10†). As shown in Fig. 2A, after incubation of **NBON** with the A549 cells for 60 min, the fluorescence signal gradually increased in intensity, reaching a maximum value at ∼40 min. This bright fluorescence signal demonstrated that **NBON** was activated by the overexpression of NADH in the A549 cells. Images were also obtained to detect exogenous NADH (0–3 mM) (Fig. 2B and C), further confirming that **NBON** can be sensitively activated by exogenous NADH during live-cell imaging.

Subsequently, the cellular distribution of **NBON** was investigated in A549 cells using the commercial agents MitoTracker Green and LysoTracker Green (Fig. 2D). Co-localization imaging results revealed enhanced **NBON** localization in the mitochondria (Pearson correlation coefficient = 0.94) compared to in the lysosomes (Pearson correlation coefficient = 0.78), likely due to the electrostatic interactions between the positively charged **NBON** and the negative potential of the inner mitochondrial membrane. These results therefore suggest that **NBON** was mainly located in mitochondria.

It is well known that the pyruvate/lactate imbalance greatly influences NADH levels in living cells,[50] wherein lactate dehydrogenase is able to efficiently catalyze the oxidation of NADH by transporting two electrons from NADH to pyruvate for the generation of lactate. Therefore, changes in NADH levels were investigated during pyruvate/lactate by using **NBON**. As shown in Fig. 3A and B, a considerably increased fluorescence signal (∼1.4-fold) was observed upon the incubation of A549 cells with exogenous lactate. In contrast, pyruvate-treated cells exhibited a large fluorescence reduction (Fig. 3B and S11†), suggesting that **NBON** can be used to detect changes in the endogenous NADH levels caused by the pyruvate/lactate imbalance in living cells.

Changes in NADH levels were subsequently evaluated in the respiratory cascade, considering the important role of NADH in mitochondrial oxidative phosphorylation during rotenone stimulation (a known respiratory complex I inhibitor). Notably, an increased fluorescence was achieved with different concentrations of rotenone (Fig. S12†), indicating that the NADH levels increased during the oxidation of complex I in the mitochondrial respiratory chain. The experiment was also performed using carbonyl cyanide chlorophenylhydrazone (CCCP)-treated cells. The uncoupler, CCCP, affects ATP synthesis by increasing the proton permeability across the inner mitochondrial membrane. The fluorescence images show an obvious decrease in the fluorescence intensity of **NBON** in the CCCP

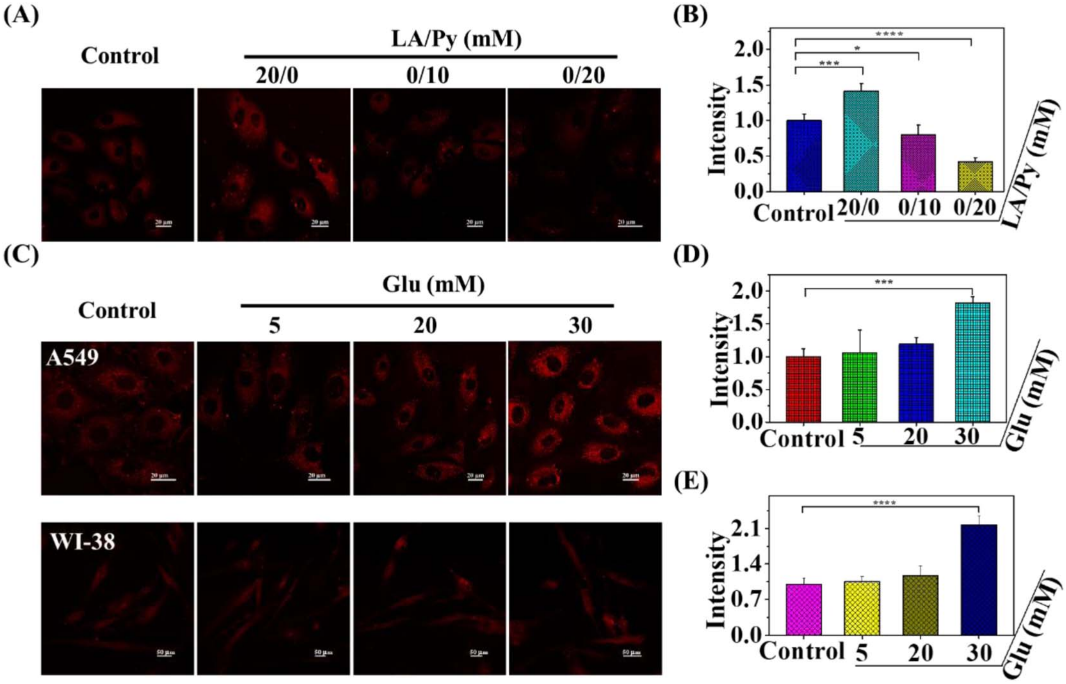

Fig. 3 (A) Fluorescence images of NADH in A549 cells treated with only probe **NBON** (15 μM) or pretreated with LA/Py (20/0, 0/10 and 0/20 mM) for 30 min. Scale bar: 20 μm. (B) Relative fluorescence intensity in (A). (C) Fluorescence images of NADH in A549 and WI-38 cells treated with only probe **NBON** (15 μM) or pretreated with glucose (5, 20 and 30 mM) for 12 h. (D and E) Relative fluorescence intensity in (C) for A549 cells (D) and for WI-38 cells (E). ($n \geq 3$, data expressed as mean ± SD, $^*P < 0.05$, $^{***}P < 0.001$ and $^{****}P < 0.0001$, Student's t-test). Scale bar: 20 μm for A549 cells and 50 μm for WI-38 cells.

Open Access Article. Published on 24 April 2025. Downloaded on 2/23/2026 1:20:25 PM.
This article is licensed under a Creative Commons Attribution-NonCommercial 3.0 Unported Licence.

dose-dependent experiment (Fig. S13†), likely due to the reduction of NADH under these conditions. Moreover, the existence of crosstalk was evaluated between the redox regulators GSH and NADH.[51] Consequently, a reduced fluorescence intensity was observed for **NBON** in the presence of high GSH concentrations (Fig. S14†), and this was attributed to the decrease in endogenous NADH levels, ultimately suggesting a close connection between the redox balance and NADH.

Fluorescence imaging of NADH in the glucose-stimulated cells

The above observations inspired the use of **NBON** to detect NADH in a diabetic disease environment. For this purpose, high glucose levels were used to stimulate cells to mimic the diabetic environment. As shown in Fig. 3C, compared to the control group, the cells pretreated with increasing doses of glucose (5, 20, and 30 mM) exhibited significantly enhanced fluorescence signals (1.1-, 1.2-, and 1.8-fold) (Fig. 3D). A similar phenomenon was observed in normal fibroblasts (WI-38) upon incubation with glucose (Fig. 3C and E). This may be due to the excessive formation of NADH during the electrochemical reduction of NAD^+ to NADH, indicating that the **NBON** probe could sensitively monitor NADH fluctuations in cells incubated with high glucose concentrations.

Under high-glucose conditions, glucose is converted into fructose through the aldose reductase (AR, a rate-limiting enzyme in the polyol pathway) and sorbitol dehydrogenase (SD, involved in oxidative stress) pathways, which can disturb the redox balance between NAD^+/NADH (Fig. 4A).[52–54] EPS, which is an AR inhibitor, can reduce the intracellular sorbitol content under high-glucose conditions, and has also been implicated in the pathogenesis of diabetic complications.[55] It was therefore speculated that EPS could alleviate or repair diabetes by inhibiting the AR enzyme and enhancing the antioxidant capacity to regulate the redox balance in living cells. Thus, experiments were conducted using living A549 and WI-38 cells. As shown in Fig. 4B, when the cells were pre-treated with different concentrations of EPS (0–50 μM) during incubation with glucose, the resulting NAD^+/NADH imbalance led to significant reductions in the **NBON** fluorescence intensity, with 6.1- and 3.3-fold reductions being observed for the A549 and WI-38 cells (*c.f.*, the strong signal obtained in the presence of glucose alone) (Fig. 4C and D). These results were attributed to

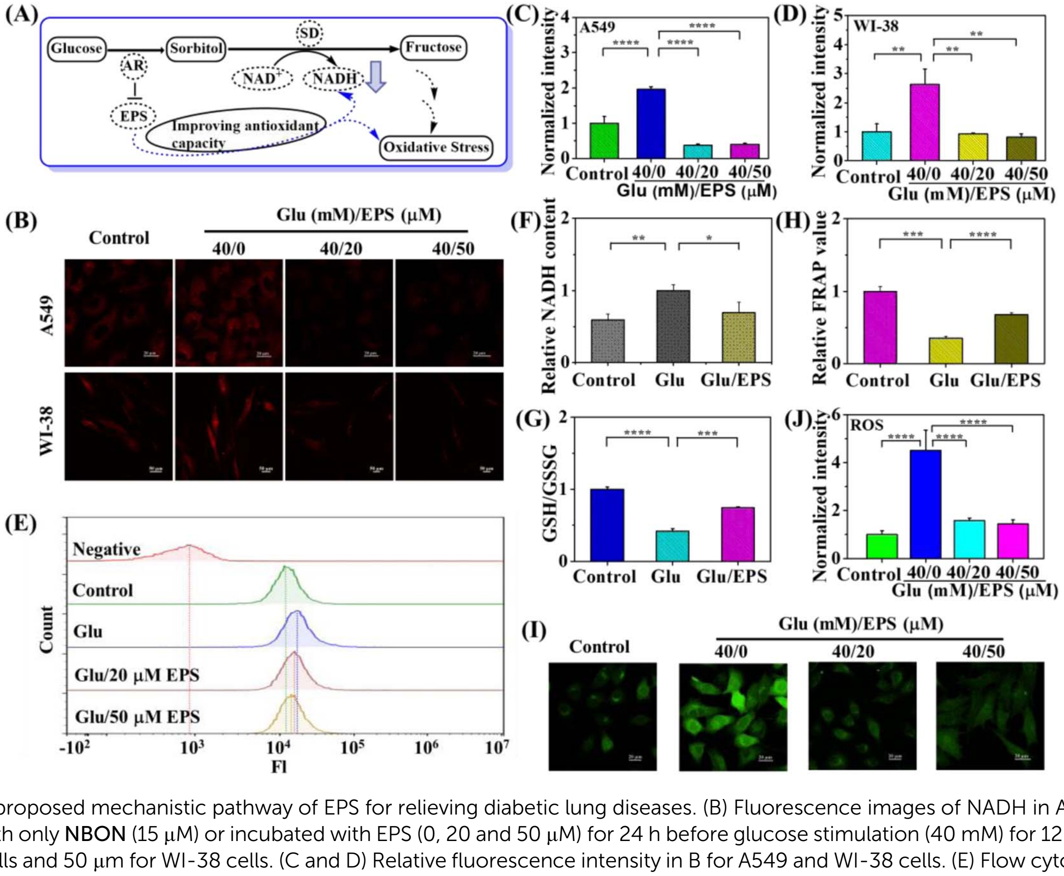

Fig. 4 (A) The proposed mechanistic pathway of EPS for relieving diabetic lung diseases. (B) Fluorescence images of NADH in A549 and WI-38 cells treated with only **NBON** (15 μM) or incubated with EPS (0, 20 and 50 μM) for 24 h before glucose stimulation (40 mM) for 12 h. Scale bar: 20 μm for A549 cells and 50 μm for WI-38 cells. (C and D) Relative fluorescence intensity in B for A549 and WI-38 cells. (E) Flow cytometric analysis of intact cells-loaded **NBON** incubated with glucose/epalrestat (40 mM/0 μM, 40 mM/20 μM and 40 mM/50 μM). (F) Measurement of NADH from cells incubated with glucose/epalrestat (40 mM/0 μM and 40 mM/50 μM). (G) Measurement of GSH/GSSG from cells incubated with glucose/epalrestat (40 mM/0 μM and 40 mM/50 μM). (H) Measurement of FRAP value from cells incubated with glucose/epalrestat (40 mM/0 μM and 40 mM/50 μM). (I) Fluorescence images of ROS in A549 treated with only commercial probe DCFH-DA (20 μM) or incubated with EPS (0, 20 and 50 μM) for 24 h before glucose stimulation (40 mM) for 12 h. Scale bar = 20 μm. (J) Relative fluorescence intensity in I. ($n \geq 3$, data expressed as mean ± SD, $^*P < 0.05$, $^{**}P < 0.01$, $^{***}P < 0.001$, and $^{****}P < 0.0001$, Student's t-test).

Open Access Article. Published on 24 April 2025. Downloaded on 2/23/2026 1:20:25 PM.
This article is licensed under a Creative Commons Attribution-NonCommercial 3.0 Unported Licence.

the downregulation of NADH under the experimental conditions. Flow cytometry was then performed (Fig. 4E), and commercial NAD^+/NADH and GSH/GSSG assay kits were employed to detect the contents of NADH and GSH/GSSG in the EPS-treated cells. It was found that the level of NADH was reduced 1.4-fold (Fig. 4F), while the GSH/GSSG level was increased 1.8-fold compared to their corresponding levels in the glucose-treated cells (Fig. 4G), thereby confirming the downregulation of NADH levels and the upregulation of GSH levels. A total antioxidant capacity assay kit based on the ferric reducing ability of plasma (FRAP) method (*i.e.*, a T-AOC Assay Kit) was also used to evaluate the redox state of the system, demonstrating an enhanced antioxidant capacity for the cells treated with EPS (Fig. 4H). Importantly, for further evaluation of the ROS and GSH levels in cells under EPS treatment conditions, experiments were also performed using a commercial ROS assay kit[56] and a GSH probe[57] that was previously reported by our group. It was found that the ROS levels decreased following EPS stimulation (Fig. 4I and J), while the GSH levels increased (Fig. S15†), thereby confirming the above findings and suggesting that EPS has the potential to relieve high glucose-induced diabetes by regulating the redox balance. Moreover, these results demonstrate that the small molecule **NBON** probe is suitable for monitoring NADH levels in living cells under these conditions.

In vivo imaging of NADH in a diabetic lung disease model

Given its impressive *in vitro* performance, the ability of **NBON** to detect NADH in a mouse model of diabetic lung disease was evaluated. Initially, the biosafety of **NBON** was assessed in healthy Kunming mice to ensure a low systemic toxicity during *in vivo* treatment. The major organs (*i.e.*, heart, liver, spleen, lungs, and kidneys) of the mice were collected for hematoxylin and eosin (H&E) staining 24 h after the intravenous injection of **NBON**. Importantly, no obvious histopathological or physiological diseases were observed in the mice treated with **NBON** (*c.f.*, the saline treatment group) (Fig. S16†). In addition, a hemolysis test was performed using **NBON**, indicating a slight change in hemolysis (Fig. S17†), and suggesting that the test dose of **NBON** exhibited a small degree of toxicity during *in vivo* imaging.

Subsequently, the biodistribution of **NBON** was examined after its intravenous administration in mice, and as shown in Fig. S18,† **NBON** was preferentially accumulated in the livers within 2 hours, and also enriched in lungs after 4.5 hours injection. The biodistribution of the NBCS product (*i.e.*, from the reaction between **NBON** and NADH) was also tracked, and it was found that NBCS was mainly localized in the lungs (Fig. 5A), while CS was mainly distributed in the liver (Fig. 5B). These results indicate that the introduction of the phenylboronic acid analog into the molecular skeleton of the CS dye promotes its accumulation in the lungs, likely due to the change in its hydrophilic/hydrophobic properties. These results indicate that the **NBON** reporter is suitable for imaging diabetic lung disease *in vivo*.

The response of **NBON** to NADH was then evaluated in mice. As shown in Fig. S19,† the signal recorded for the right thigh, which was stimulated with exogenous NADH, clearly increased compared to that observed for the left thigh, which was treated only with **NBON**. This result reveals the potential of **NBON** for detecting NADH *in vivo*. Subsequently, the ability of **NBON** to visualize changes in the NADH level was evaluated in a mouse diabetic lung disease model (Fig. 5C). To the best of our knowledge, direct evidence for NADH generation in this context is lacking. Thus, a diabetic lung disease model was constructed using streptozotocin (STZ)[58] to image endogenous NADH generation. Metformin (MET), a biguanide derivative,[58] was selected as the traditional medication for diabetes, and EPS was also used to evaluate its therapeutic effects in diabetes based on its excellent performance in living cells. The experiments were divided into four groups, namely the control (PBS treatment only), STZ, STZ/MET, and STZ/EPS groups. As shown in Fig. 5D, the mice in the control group showed no fluorescence signal. For the STZ group, the mice from were intraperitoneally injected with STZ over 7 days following the intravenous injection of **NBON** (100 μL, 200 μM). Consequently, the fluorescence signals in the mice lungs gradually increased (1.8-, 1.9-, and 2.0-fold, respectively) at time intervals (30, 90, and 150 min) compared with the mice of the control group (Fig. 5E). This result was mainly attributed to the NAD^+/NADH imbalance in the STZ-stimulated mice, which resulted in excessive NADH formation, as demonstrated using the commercial NAD^+/NADH kit (Fig. 5F). In living systems, a NAD^+/NADH imbalance is known to affect the antioxidant capacity of the organism. It was therefore speculated that compared to the control group, the antioxidant capacities of the tissues would be significantly reduced under STZ stimulation, as demonstrated using the T-AOC assay kit (Fig. 5G). Notably, when mice from the STZ/MET and STZ/EPS groups were treated with MET for 28 d and EPS for 49 d, respectively, maximum reductions of 2.0- and 2.1-fold were observed for the fluorescence signals of the lungs in the STZ/MET and STZ/EPS groups. These results were attributed to recovery of the NAD^+/NADH balance in the lung after MET and EPS treatment for diabetic lung disease, resulting in lower NADH levels (Fig. 5F) and an enhanced antioxidant capacity (Fig. 5G). Moreover, H&E staining revealed different pathological characteristics before and after treatment of the lung injury (Fig. 5H), which were supported by an *ex vivo* organ experiment performed in the presence of **NBON** (Fig. 5I and S20†). Taken together, these results imply that EPS has the potential to treat diabetic lung disease based on its regulation of the system redox state, thereby demonstrating that the probe **NBON** is applicable for the high-fidelity imaging of lung disease and repair *in vivo*.

In vivo imaging of NADH for lung metastases and tumors

The worst-case outcome of lung disease is the development of lung tumors, which primarily include metastatic and primary tumors. Based on the favorable properties of **NBON** identified above, investigations were carried out to assess its performance in the imaging of lung metastases and tumors in mice. For this purpose, the mice were divided into two groups, namely normal mice and mice with lung metastases. More specifically, BALB/c mice with lung metastases were established by the intravenous

Open Access Article. Published on 24 April 2025. Downloaded on 2/23/2026 1:20:25 PM.
This article is licensed under a Creative Commons Attribution-NonCommercial 3.0 Unported Licence.

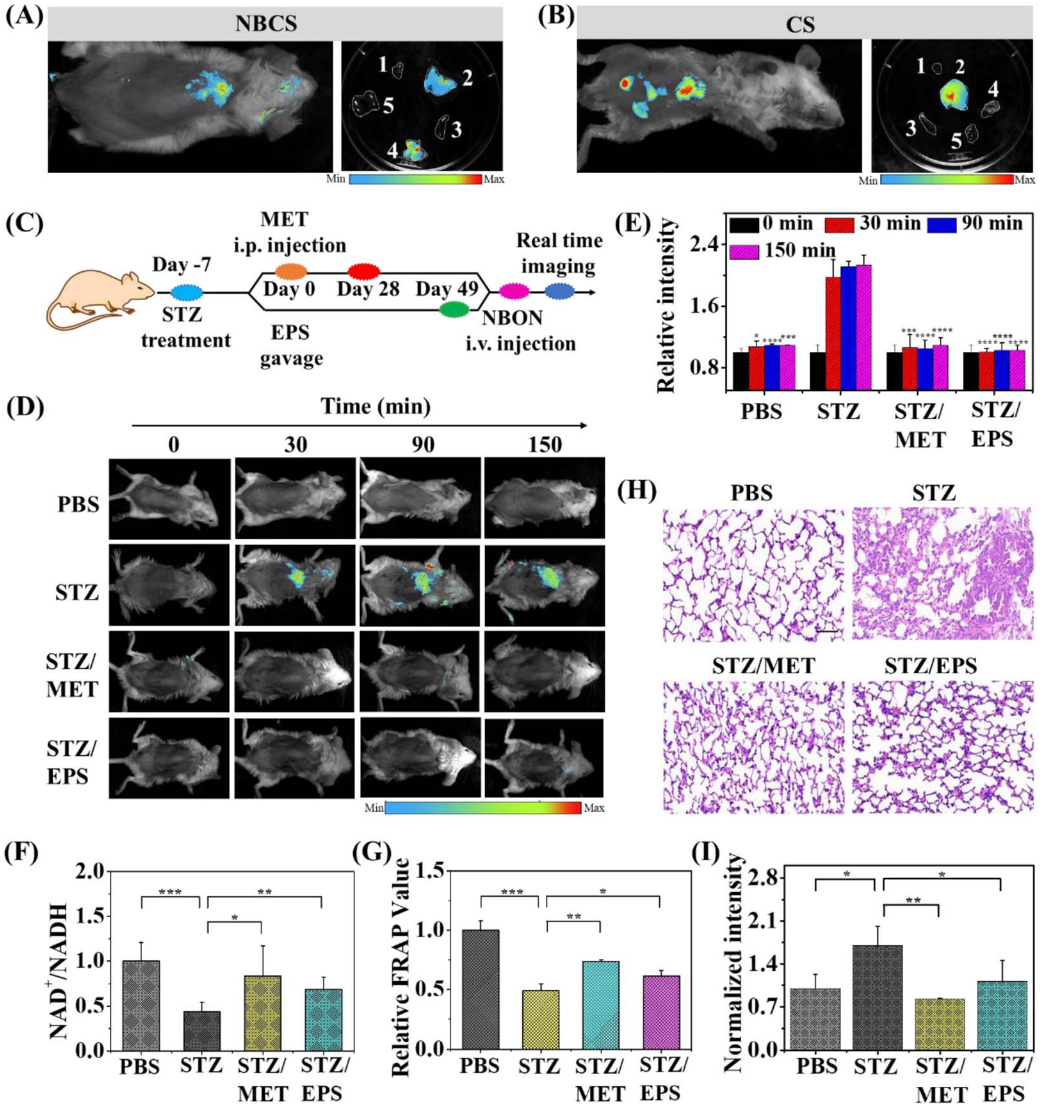

Fig. 5 Fluorescence images of compounds NBCS (A) and CS (B) in mice (intravenous injection, 60 μL, 200 μM, 90 min) and *ex vivo*. (1) Heart; (2) liver; (3) spleen; (4) lung; (5) kidney. (C) Schematic representation for constructing diabetic lung disease model and imaging. (D) Real-time imaging of Kunming mice with different treatment by receiving injection of PBS, STZ (150 mg kg^{-1}, intraperitoneal), STZ/MET (150/200 mg kg^{-1}, intraperitoneal) and STZ/EPS (150/100 mg kg^{-1}, intraperitoneal/gavage), followed by intravenously injecting **NBON** (60 μL, 200 μM). (E) Relative fluorescence intensity in D. (F) Measurement of NAD^+/NADH ratio and (G) FRAP value of lung tissues from mice treated with STZ (150 mg kg^{-1}), STZ/MET (150/200 mg kg^{-1}) and STZ/EPS (150/100 mg kg^{-1}). (H) Hematoxylin and eosin (H&E) staining of lung tissues from mice treated with STZ (150 mg kg^{-1}), STZ/MET (150/200 mg kg^{-1}) and STZ/EPS (150/100 mg kg^{-1}). Scale bar: 50 μm. (I) Normalized intensity for the lung incubated with **NBON** from mice treated with STZ (150 mg kg^{-1}), STZ/MET (150/200 mg kg^{-1}) and STZ/EPS (150/100 mg kg^{-1}). ($n = 3$, data expressed as mean ± SD, $*P < 0.05$, $**P < 0.01$, $***P < 0.001$, and $****P < 0.0001$, Student's *t*-test).

injection of 4T1 cells for three weeks (Fig. 6A). Subsequently, these mice were intravenously injected with **NBON** (100 μL, 200 μM), and as shown in Fig. 6B, apparent signal enhancements were observed in the metastasis group over time (*i.e.*, at 25 and 120 min), whereas a negligible signal change was observed for the normal mice. After sacrifice, lung samples were collected from the mice (Fig. 6B(c) and 6B(g)), and the *ex vivo* fluorescence images also showed a large difference in the signal intensity between the two groups (Fig. 6B(d) and 6B(h)). More specifically, cancer cell metastases were only observed on the lung tissue surfaces of the mice with lung metastasis; no changes were observed for the normal lungs. These results were further verified by H&E staining (Fig. 6C), which indicated that **NBON** can track metastatic lung tumor lesions and image NADH levels during lung metastasis *in vivo*. Finally, an additional experiment was conducted using **NBON** to image NADH and guide the resection of lung tumors. The tumor model was established by implanting A549 cells into BALB/c mice for 20 d. PBS and **NBON** (30 μL, 100 μM) were then simply sprayed onto the tumor (Fig. S21†). Notably, the tumor was accurately lit up *in situ* within 25 min, while no fluorescence signal was obtained after spraying with PBS alone (Fig. 6D). Consequently, it was

© 2025 The Author(s). Published by the Royal Society of Chemistry

Open Access Article. Published on 24 April 2025. Downloaded on 2/23/2026 1:20:25 PM.
This article is licensed under a Creative Commons Attribution-NonCommercial 3.0 Unported Licence.

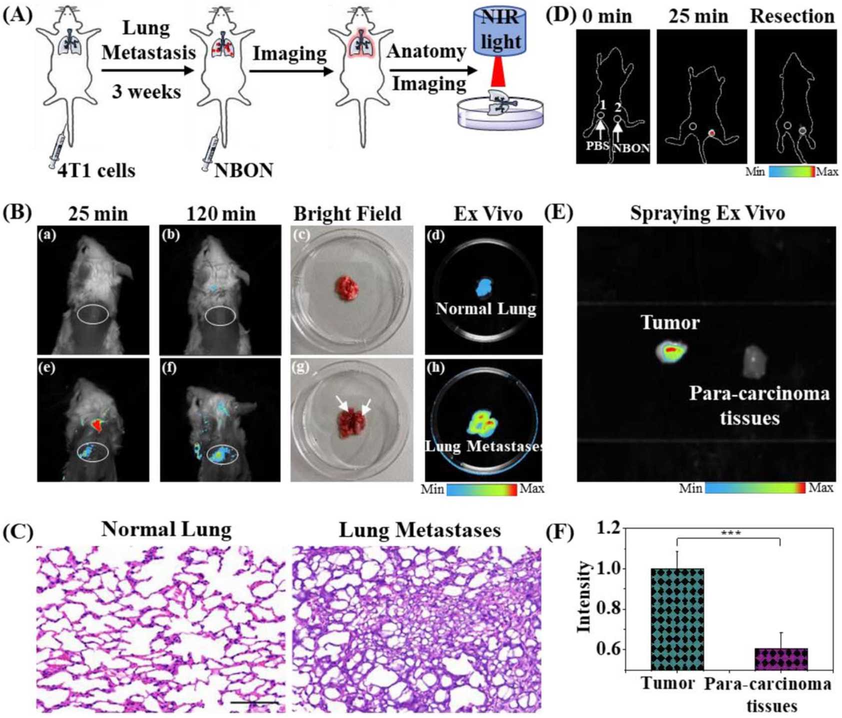

Fig. 6 (A) Schematic representation for lung metastatic tumor model and imaging. (B) Imaging of normal lung (first row) and lung metastatic tumor (second row) through intravenously injecting **NBON** (100 μL, 200 μM) in BALB/c mice. White oval: lung. (a and e) Injecting intravenously **NBON** for 25 min, then fluorescence image; (b and f) injecting intravenously **NBON** for 120 min, then fluorescence image; (c and g) bright image (up: normal lung; down: lung metastasis); (d and h) dissection lung tissues from BALB/c mice after injecting intravenously **NBON** for 130 min. (C) Hematoxylin and eosin (H&E) staining of normal lung and lung metastasis from mice. Scale bar: 50 μm. (D) Fluorescence-guided resection and imaging of lung tumor through spraying PBS and **NBON** (30 μL, 100 μM) in BALB/c mice. 1 and 2: lung tumor for PBS (1) and **NBON** (2). (E) Imaging of lung tumor and para-carcinoma tissues through spraying **NBON** (10 μL, 500 μM) *ex vivo*. (F) Relative intensity in (E). ($n = 3$, data expressed as mean ± SD, $^{***}P < 0.001$, Student's t-test).

possible to completely remove the tumor under the fluorescence guidance provided by **NBON** (Fig. 6D). Additionally, *in vitro* lung tumor and para-carcinoma tissues could also be effectively distinguished *via* the *in situ* spraying of **NBON** at a tumor/normal tissue ratio of 1.7 : 1 (Fig. 6E and F). These results confirm the potential of **NBON** for NADH detection/imaging in lung tumors, and its role in aiding in the accurate resection of lung tumors.

Conclusions

In summary, a lung-targeted nicotinamide adenine dinucleotide (NADH)-sensitive long-wavelength near-infrared (NIR) fluorescent reporter (**NBON**) was designed and developed using a tandem reaction (TR) strategy based on the dual reactions of NADH. More specifically, a group containing a phenylboronic acid analog was initially attached onto a probe molecule to promote an esterification-crosslinking reaction with the adjacent diols present in the NADH structure. Subsequently, the recognition group on the probe molecule was modified for reduction by NADH, rendering it highly reactive and leading to a strong fluorescence signal in the presence of NADH. This approach generated a sensitive probe with a low NADH detection limit (45 nM), and which also selectively accumulated in the lung. Importantly, these characteristics indicated the potential of the **NBON** for detecting the NADH generated in diabetic lung disease. Owing to the high sensitivity and selectivity observed for **NBON** *in vitro*, it was subsequently confirmed that this probe could detect small fluctuations in the NADH levels in living cells during high-glucose stimulations and epalrestat (EPS) repair. In addition, **NBON** was above to track changes in the NADH levels in streptozotocin-induced diabetic lung injury and MET/EPS repair models in mice. More importantly, the proposed antioxidant mechanism by which EPS alleviates diabetic lung disease was confirmed for the first time in living cells and *in vivo*. Finally, the endogenous NADH present in lung tumors and metastases was successfully monitored using **NBON**, and its role in aiding in the accurate resection of lung tumors was demonstrated. It is expected that this novel TR strategy will be applicable to the development other activatable probes. Moreover, this work should promote further research into the design of NADH probes for biological applications, including disease diagnosis and therapy.

Data availability

The data supporting this article have been included in the ESI.† Additional data are available upon request from the corresponding author. All animal procedures were performed in accordance with the Guide for the Care and Use of Laboratory

Open Access Article. Published on 24 April 2025. Downloaded on 2/23/2026 1:20:25 PM.
This article is licensed under a Creative Commons Attribution-NonCommercial 3.0 Unported Licence.

Animals, and were approved (approval number: No. SYXK (Xiang) 2020-0002) by University of South China.

Author contributions

Y. Hu, H. Zhang and Y. Ding: data curation, methodology, investigation, and visualization. W. Chen: investigation, data curation, methodology, and visualization. C. Pan: resources. L. He: conceptualization, writing – review and editing, resources and funding acquisition. D. Cheng and L. Yuan: conceptualization, writing – review and editing, resources and funding acquisition. All authors discussed the results and assisted during manuscript preparation.

Conflicts of interest

There are no conflicts to declare.

Acknowledgements

This work was supported by the National Natural Science Foundation of China (22074036), the Science and Technology Project of Hunan Province (2021RC3108), the Hunan Provincial Natural Science Foundation of China (2022JJ10042, 2022JJ30484, 2023JJ40412), the Special Funding for the Construction of Innovative Provinces in Hunan (2021SK4031).

Notes and references

1 M. Brownlee, *Nature*, 2001, **414**, 813–820.
2 S. Amanat, S. Ghahri, A. Dianatinasab, M. Fararouei and M. Dianatinasab, *Adv. Exp. Med. Biol.*, 2020, **1228**, 91–105.
3 N. H. Cho, J. E. Shaw, S. Karuranga, Y. Huang, J. D. da Rocha Fernandes, A. W. Ohlrogge and B. Malanda, *Diabetes Res. Clin. Pract.*, 2018, **138**, 271–281.
4 M. R. Schuyler, D. E. Niewoehner, S. R. Inkley and R. Kohn, *Am. Rev. Respir. Dis.*, 1976, **113**, 37–41.
5 D. Pitocco, L. Fuso, E. G. Conte, F. Zaccardi, C. Condoluci, G. Scavone, R. A. Incalzi and G. Ghirlanda, *Rev. Diabet. Stud.*, 2012, **9**, 23–35.
6 S. F. Ehrlich, C. P. Quesenberry, S. K. Van Den Eeden, J. Shan and A. Ferrara, *Diabetes Care.*, 2010, **33**, 55–60.
7 S. S. Garg and J. Gupta, *Pharmacol. Res.*, 2022, **182**, 106326.
8 J. Wu, Z. Jin and L. J. Yan, *Redox Biol.*, 2017, **11**, 51–59.
9 D. Cheng, J. Peng, Y. Lv, D. Su, D. Liu, M. Chen, L. Yuan and X. Zhang, *J. Am. Chem. Soc.*, 2019, **141**, 6352–6361.
10 H. Chang, S. Clemens, P. Gao, Q. Li, H. Zhao, L. Wang, J. Zhang, P. Zhou, K. Johnsson and L. Wang, *J. Am. Chem. Soc.*, 2024, **146**, 20569–20576.
11 Y. Xu, C. Li, S. Lu, Z. Wang, S. Liu, X. Yu, X. Li and Y. Sun, *Nat. Commun.*, 2022, **13**, 2009.
12 Z. Wang, W. Wang, P. Wang, X. Song, Z. Mao and Z. Liu, *Anal. Chem.*, 2021, **93**, 3035–3041.
13 X. Wu, W. Shi, X. Li and H. Ma, *Acc. Chem. Res.*, 2019, **52**, 1892–1904.
14 Z. Yuwen, Q. Zeng, Q. Ye, Y. Zhao, J. Zhu, K. Chen, H. Liu and R. Yang, *Angew. Chem., Int. Ed.*, 2023, **135**, e202302957.
15 X. Zhang, F. Yang, T. Ren, Y. Zheng, X. Zhang and L. Yuan, *Chin. Chem. Lett.*, 2023, **34**, 107835.
16 Q. Liu, J. Yuan, R. Jiang, L. He, X. Yang, L. Yuan and D. Cheng, *Anal. Chem.*, 2023, **95**, 2062–2070.
17 B. Hu, Q. Liu, Y. Jiang, Y. Huang, H. Ji, J. Zhang, X. Wang, X.-C. Shen and H. Chen, *Angew. Chem., Int. Ed.*, 2025, **64**, e202418378.
18 X. Wang, S. S. Liew, J. Huang, Y. Hu, X. Wei and K. Pu, *J. Am. Chem. Soc.*, 2024, **146**, 22689–22698.
19 M. Vendrell, D. Zhai, J. C. Er and Y. T. Chang, *Chem. Rev.*, 2012, **112**, 4391–4420.
20 D. Cheng, W. Xu, X. Gong, L. Yuan and X. B. Zhang, *Acc. Chem. Res.*, 2021, **54**, 403–415.
21 Z. Mao, J. Xiong, P. Wang, J. An, F. Zhang, Z. Liu and J. S. Kim, *Coord. Chem. Rev.*, 2022, **454**, 214356.
22 R. Wu, Z. Chen, H. Huo, L. Chen, L. Su, X. Zhang, Y. Wu, Z. Yao, S. Xiao, W. Du and J. Song, *Anal. Chem.*, 2022, **94**, 10797–10804.
23 Y. Xu, W. Tuo, L. Yang, Y. Sun, C. Li, X. Chen, W. Yang, G. Yang, P. J. Stang and Y. Sun, *Angew. Chem., Int. Ed.*, 2022, **61**, e202110048.
24 J. Chan, S. C. Dodani and C. J. Chang, *Nat. Chem.*, 2012, **4**, 973–984.
25 L. Wang, J. Zhang, B. Kim, J. Peng, S. N. Berry, Y. Ni, D. Su, J. Lee, L. Yuan and Y. T. Chang, *J. Am. Chem. Soc.*, 2016, **138**, 10394–10397.
26 Y. Zhao, K. Wei, F. Kong, X. Gao, K. Xu and B. Tang, *Anal. Chem.*, 2019, **91**, 1368–1374.
27 X. Pan, Y. Zhao, T. Cheng, A. Zheng, A. Ge, L. Zang, K. Xu and B. Tang, *Chem. Sci.*, 2019, **10**, 8179–8186.
28 A. Podder, S. Koo, J. Lee, S. Mun, S. Khatun, H. G. Kang, S. Bhuniya and J. S. Kim, *Chem. Commun.*, 2019, **55**, 537–540.
29 R. Freeman, R. Gill, I. Shweky, M. Kotler, U. Banin and I. Willner, *Angew. Chem., Int. Ed.*, 2009, **48**, 309–313.
30 K. Ma, H. Yang, X. Wu, F. Huo, F. Cheng and C. Yin, *Angew. Chem., Int. Ed.*, 2023, **62**, e202301518.
31 J. Joo, D. Youn, S. Park, D. Shin and M. Lee, *Dyes Pigm.*, 2019, **170**, 107561.
32 L. Yuan, W. Lin, K. Zheng, L. He and W. Huang, *Chem. Soc. Rev.*, 2013, **42**, 622–661.
33 H. Li, H. Kim, F. Xu, J. Han, Q. Yao, J. Wang, K. Pu, X. Peng and J. Yoon, *Chem. Soc. Rev.*, 2022, **51**, 1795–1835.
34 E. A. Owens, M. Henary, G. El Fakhri and H. S. Choi, *Acc. Chem. Res.*, 2016, **49**, 1731–1740.
35 H. Li, Y. Kim, H. Jung, J. Y. Hyun and I. Shin, *Chem. Soc. Rev.*, 2022, **51**, 8957–9008.
36 C. Li, Y. Pang, Y. Xu, M. Lu, L. Tu, Q. Li, A. Sharma, Z. Guo, X. Li and Y. Sun, *Chem. Soc. Rev.*, 2023, **52**, 4392–4442.
37 J. Weng, Z. Huang, Y. Liu, X. Wen, Y. Miao, J. J. Xu and D. Ye, *J. Am. Chem. Soc.*, 2024, **146**, 13163–13175.
38 J. Liu, W. Zhang, C. Zhou, M. Li, X. Wang, W. Zhang, Z. Liu, L. Wu, T. D. James, P. Li and B. Tang, *J. Am. Chem. Soc.*, 2022, **144**, 13586–13599.
39 S. S. Liew, Z. Zeng, P. Cheng, S. He, C. Zhang and K. Pu, *J. Am. Chem. Soc.*, 2021, **143**, 18827–18831.
40 Y. Ding, R. Zhong, R. Jiang, X. Yang, L. He, L. Yuan and D. Cheng, *ACS Sens.*, 2023, **8**, 914–922.

© 2025 The Author(s). Published by the Royal Society of Chemistry

Open Access Article. Published on 24 April 2025. Downloaded on 2/23/2026 1:20:25 PM.
This article is licensed under a Creative Commons Attribution-NonCommercial 3.0 Unported Licence.

41 W. Zhang, T. Chen, L. Su, X. Ge, X. Chen, J. Song and H. Yang, *Anal. Chem.*, 2020, **92**, 6094–6102.
42 K. Li, Y. Lyu, Y. Huang, S. Xu, H. W. Liu, L. Chen, T. B. Ren, M. Xiong, S. Huan, L. Yuan, X. B. Zhang and W. Tan, *Proc. Natl. Acad. Sci. U. S. A.*, 2021, **118**, e2018033118.
43 R. Zhong, R. Jiang, J. Zeng, X. Gong, X. Yang, L. He, L. Yuan and D. Cheng, *Anal. Chem.*, 2023, **95**, 2428–2435.
44 J. Liu, W. Zhang, C. Zhou, M. Li, X. Wang, W. Zhang, Z. Liu, L. Wu, T. D. James, P. Li and B. Tang, *J. Am. Chem. Soc.*, 2022, **144**, 13586–13599.
45 S. Zhang, H. Chen, L. Wang, X. Qin, B. P. Jiang, S. C. Ji, X. C. Shen and H. Liang, *Angew. Chem., Int. Ed.*, 2022, **61**, e202107076.
46 D. Cheng, Y. Pan, L. Wang, Z. Zeng, L. Yuan, X. Zhang and Y. T. Chang, *J. Am. Chem. Soc.*, 2017, **139**, 285–292.
47 H. Bian, D. Ma, F. Pan, X. Zhang, K. Xin, X. Zhang, Y. Yang, X. Peng and Y. Xiao, *J. Am. Chem. Soc.*, 2022, **144**, 22562–22573.
48 Y. Wei, D. Cheng, T. Ren, Y. Li, Z. Zeng and L. Yuan, *Anal. Chem.*, 2016, **88**, 1842–1849.
49 J. S. Brody, C. A. Vaccaro, N. S. Hill and S. Rounds, *Circ. Res.*, 1984, **55**, 155–167.
50 Y. P. Hung and G. Yellen, *Cell Metab.*, 2014, **1071**, 83–95.
51 C. Busu, V. Atanasiu, G. Caldito and T. Y. Aw, *J. Med. Life*, 2014, **7**, 611–618.
52 T. F. Ng, F. K. Lee, Z. T. Song, N. A. Calcutt, A. Y. Lee, S. S. Chung and S. K. Chung, *Diabetes*, 1998, **47**, 961–966.
53 A. Y. Lee and S. S. Chung, *FASEB J.*, 1999, **13**, 23–30.
54 J. Wu, Z. Jin, H. Zheng and L. J. Yan, *Diabetes, Metab. Syndr. Obes.: Targets Ther.*, 2016, **9**, 145–153.
55 J. W. Steele, D. Faulds and K. L. Goa, *Drugs Aging*, 1993, **3**, 532–555.
56 H. Hao, L. Cao, C. Jiang, Y. Che, S. Zhang, S. Takahashi, G. Wang and F. J. Gonzalez, *Cell Metab.*, 2017, **25**, 856–867.
57 R. Jiang, H. Zhang, Q. Liu, X. Yang, L. He, L. Yuan and D. Cheng, *Adv. Healthcare Mater.*, 2024, **13**, 2302466.
58 S. Li, K. Yang, Y. Liu, P. Wang, D. Cheng and L. He, *Sens. Actuators, B*, 2023, **379**, 133253.

© 2025 The Author(s). Published by the Royal Society of Chemistry